Template-Assisted Large-Scale Ordered Arrays of ZnO Pillars for Optical and Piezoelectric Applications

Hong Jin Fan,* Woo Lee, Robert Hauschild, Marin Alexe, Gwenaël Le Rhun, Roland Scholz, Armin Dadgar, Kornelius Nielsch, Heinz Kalt, Alois Krost, Margit Zacharias, and Ulrich Gösele

Spatially separated ZnO pillars, typically 300 nm in diameter and 2 μm in height, are fabricated via a template-directed approach that leads to long-range hexagonal order. The templates of Au nanodisk arrays are obtained by using metal membranes as a lithography mask. The growth of ZnO pillars is performed in a double-tube system through vapor diffusion–deposition. The growth mechanism of the pillars is studied in detail and is proposed to be a combination of vapor–liquid–solid and vapor–solid models. The piezoelectric and optical properties of single pillars are characterized using piezoresponse force microscopy and micro-photoluminescence spectroscopy, respectively. The pillars show strong excitonic emissions up to room temperature, which indicate a relatively low defect density and good crystalline quality. The obtained piezoelectric coefficient d_{33} is (7.5 ± 0.6) pm V^{-1}, which is to our knowledge the first reported value for a single nanopillar.

Keywords:
· actuators
· nanowires
· photoluminescence
· piezoelectrics
· template synthesis

1. Introduction

ZnO-based quasi-one-dimensional (quasi-1D) materials have received increasing attention over the past few years due to their potential as building blocks for nanoscale photonic and sensing devices, and for applications such as piezoelectric actuators.[1] A number of publications report the fabrication of ZnO 1D nanostructures (e.g., nanowires) aligned perpendicular to the substrate in a more or less dis-

ordered spatial arrangement. For example, metal-catalyst-directed growth on epitaxial substrates,[2] growth by chemical vapor deposition[3] or by metal–organic vapor-phase epitaxy (MOVPE),[4] and growth by catalyst-free self-assembly onto different types of seed layers, such as colloidal ZnO nanoparticles,[5] undoped or doped ZnO films,[6] or GaN epilayers,[7] were demonstrated. In particular, catalyst-assisted growth is a common method for the bottom-up fabrication of such vertically aligned nanowires, which might offer the advantage of growth at specific sites. A nanopatterned metal catalyst is then mandatory. A template-based process holds the promise of large-scale and cost-effective fabrication. Different types of templates for nanopatterning were reported including porous anodic aluminum oxide (AAO) templates,[8] self-assembly nanosphere lithography,[9] and soft photolithography.[10]

For certain applications such as stimulated emitters and lasing cavities, ZnO wires with diameters in the range of 150–500 nm are more suitable than sub-150-nm nanowires. With thicker wires, a lower threshold laser action can be

[*] Dr. H. J. Fan, Dr. W. Lee, Dr. M. Alexe, Dr. G. Le Rhun,
Dr. R. Scholz, Dr. K. Nielsch, Dr. M. Zacharias, Prof. U. Gösele
Max Planck Institute of Microstructure Physics
Weinberg 2, 06120 Halle (Germany)
Fax: (+49) 345-5511-223
E-mail: hjfan@mpi-halle.de
R. Hauschild, Prof. H. Kalt
Institute of Applied Physics, University of Karlsruhe
76131 Karlsruhe (Germany)
Dr. A. Dadgar, Prof. A. Krost
Institute of Experimental Physics, Otto-von-Guericke University
39016 Magdeburg (Germany)

maintained due to the higher Q-factor resonator and the enhanced overlap of the guide modes with the gain medium. Herein, we report on the fabrication of large-area ordered arrays of ZnO pillars on GaN substrates by a template-assisted approach, which has been previously applied for the fabrication of nanowire arrays. Here we call the nanostructures "pillars" because of their vertical alignment on the substrate surface and their larger diameters (300 nm) compared with those of the nanowires we presented previously (<120 nm).[2c] These pillars exhibit an overall hexagonal ordering and narrow size distribution. Our observations reveal that the pillars do not grow exclusively through the classical vapor–liquid–solid (VLS) model, even though the presence of gold was a necessary precondition for successful position control during growth. A detailed discussion of the growth process will be presented. The optical quality of the pillars will be proven by micro-photoluminescence (micro-PL) measurements (including continuous-wave (cw) and time-resolved measurements). Furthermore, our new sample design (free-standing vertical pillars on a conductive GaN substrate) enables us to study the piezoelectric properties of single ZnO pillars using piezoresponse force microscopy (PFM). The piezoelectric characterization of [0001]-oriented ZnO thin films[11] and [$2\bar{1}\bar{1}0$]-oriented nanobelts has been published,[12] but so far there is no report on individual vertically aligned, [0001]-elongated, ZnO quasi-1D nanostructures.

2. Results and Discussion

2.1. Fabrication of the Pillar Array

The fabrication process involves a novel type of flexible metal nanotube membrane,[13] Au nanodisk arrays obtained by using the membrane as a deposition mask, and the subsequent site-specific growth of ZnO nanowires (see Experimental Section). The scanning electron microscopy (SEM) image in Figure 1 shows the deposited Au nanodisk array together with a remaining part of the membrane mask on the right-hand side. The mask has an inner nanotube diameter of ≈130 nm and an intertube distance of 500 nm. After the mask membrane was completely removed, the resulting Au nanodisk array was used as a template for subsequent growth of ZnO. Figure 2a shows a top view of the ZnO pillar arrays grown at $T_{source} = 950\,°C$ (temperature of the source) and $T_{sub} = 800\,°C$ (temperature of the substrate) for 40 min. As can be seen, the pillars are hexagonally arranged on the substrate, and have the same arrangement as the initial gold nanodisks. The magnified top view in Figure 2b and the corresponding tilted view in Figure 2c reveal that the pillars are oriented perpendicular to the substrate surface with hexagonal ends, which indicates that their main axis is oriented along [0001]. The nearest-neighbor spacing of the pillars is 500 nm, as predefined by the tube-to-tube distance of the shadow mask. The pillars have a typical height of 2 µm and a narrow size distribution centered at 300 nm (see inset in Figure 2a), which is much larger than
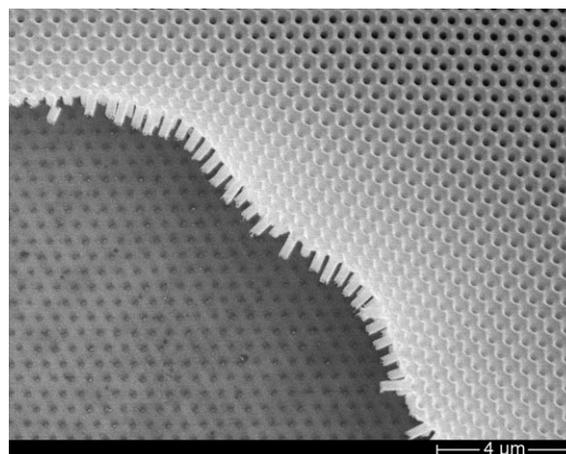

Figure 1. SEM image of the substrate surface after thermal deposition of Au using a metal nanotube membrane as a shadow mask. Part of the membrane was removed (left), thus exposing the Au nanodisk array.
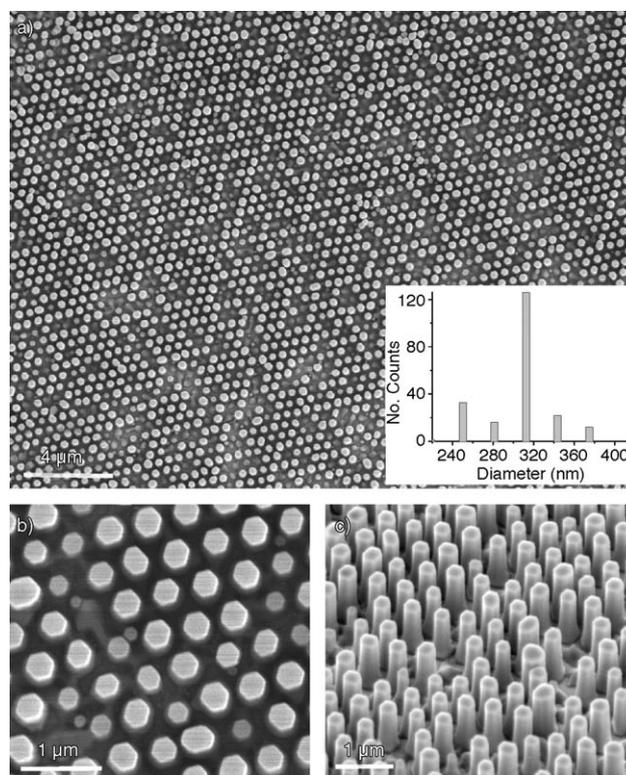

Figure 2. a) Low-magnification top view of the ZnO pillar array. Inset: diameter distribution of the pillars. b) Enlarged top view of part of the pillar array, and c) the corresponding perspective view.

expected from the deposited Au disk diameter of about 130 nm.

The long-range periodic order (up to mm²) of the pillars demonstrates the suitability of the metal nanotube membrane mask. The membranes, electrochemically replicated from an AAO master template, are flexible and easy to handle, thus assuring high fidelity of the pattern transfer.[13] Chik et al.[8] reported a similar template-directed growth of

ZnO nanorod arrays when using an AAO membrane directly as a shadow mask for Au deposition. However, due to their stiffness and hydrophilicity, such AAO membranes allow only an inhomogeneous pattern transfer on a μm^2-sized area with the inevitable occurrence of large voids in the pattern. Consequently, the nanowire arrays can only be obtained on a much smaller scale. Another benefit of our method is the long-range monodomain ordering of the resulting ZnO pillars, as well as of the nanowires reported before,[2c] while the nanorods reported by Chik et al. seem to show only a polydomain ordering.

Figure 3a shows a cross-sectional transmission electron microscopy (TEM) image of the pillars on a GaN/Si substrate. The selected electron diffraction pattern (see Fig-
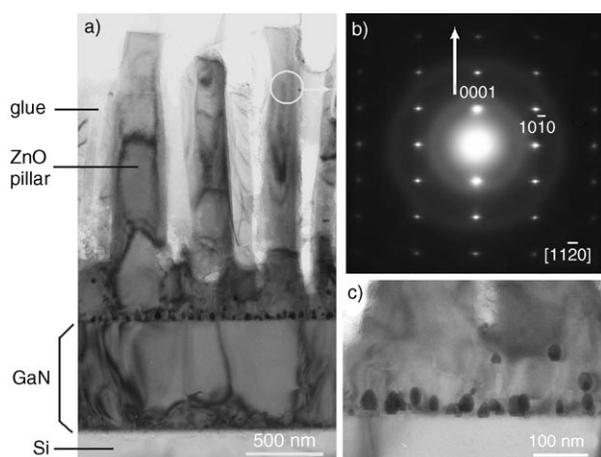

Figure 3. a) Cross-sectional TEM image of the ZnO pillars. b) Electron diffraction pattern taken from the area of the pillar body circled in (a). The arrow indicates the main axis direction of the pillars. c) Magnified view of the interface of ZnO pillars and GaN showing the Au particles. Note that the curvature of the pillars is caused by the glue used during TEM sample preparation.

ure 3b) verifies that the pillars are single crystalline and grow along [0001]. Note that the ripple-like contrast of the pillars is not related to grain boundaries but rather to bending due to the glue used for TEM sample preparation. Some of the pillars are interconnected at their bases by a crystalline ZnO layer, as seen in Figure 2c and exemplified by Figure 3a. A careful examination of the ZnO pillar/GaN film interface reveals the existence of a layer of particles that stay mostly on the GaN surface (Figure 3c). The particles were confirmed to be Au by high-resolution TEM investigations. The Au particles also appear to be almost homogeneously distributed at locations initially not covered by Au.

2.2. The Growth Mechanism

The classical VLS mechanism[14] has been widely used for bottom-up fabrication of semiconductor whiskers[1,15] and nanowires, including ZnO.[9] In this mechanism, the catalytic Au particles normally stay at the growth fronts of the materials, that is, atop the pillars. In our case, the Au nano-

disk array directed the growth of ZnO pillars. However, the post-growth TEM analysis revealed that the Au does not appear at the top ends of the pillars but at the base in the form of Au dots with diameters much smaller than those of the ZnO pillars (see Figure 3). In addition, the pillar diameter of 300 nm is more than double the size of the initial gold disks (130 nm). These findings indicate that the mechanism governing the growth of such large-diameter pillars under our experimental conditions is not a simple VLS process.

Time-sequenced growth experiments were conducted to shed light on the growth mechanism. Figure 4 shows the
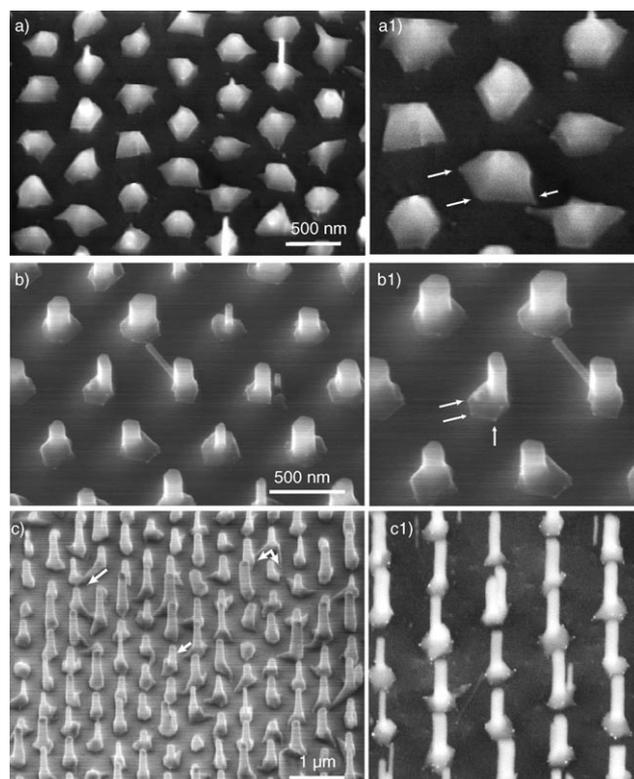

Figure 4. Perspective-view SEM images representing the early growth stages of the ZnO pillar. a) Sample surface after <1 min growth. b) Sample surface after 5 min growth. c) Pillars with diameters of ≈180 nm and length of 1 μm after 20 min growth. The arrows indicate the lateral growth of ZnO on the substrate surface. Right-hand column: the corresponding enlarged SEM images showing the Au nanoparticles surrounding the ZnO nuclei (see arrows in (a1) and (b1)) or the short pillars (white spots in (c1)).

sample surface after growth using the same conditions (viz., $T_{source} = 950\,°C$, $T_{sub} = 800\,°C$) except for different growth times, which were chosen to represent the various growth stages of the pillars. The schematic diagram in Figure 5 illustrates the proposed growth process. Figure 4a shows the result after <1 min growth, that is, the furnace was switched off immediately when the temperature reached the peak value (950°C). An array of alloyed points, ≈250 nm in width, was observed at the catalyst sites. At the high-temperature end (i.e., closed end) of the small tube, Zn vapor was produced by the reaction of ZnO powder with graphite and carbon monoxide[2d,16] and diffused toward the open
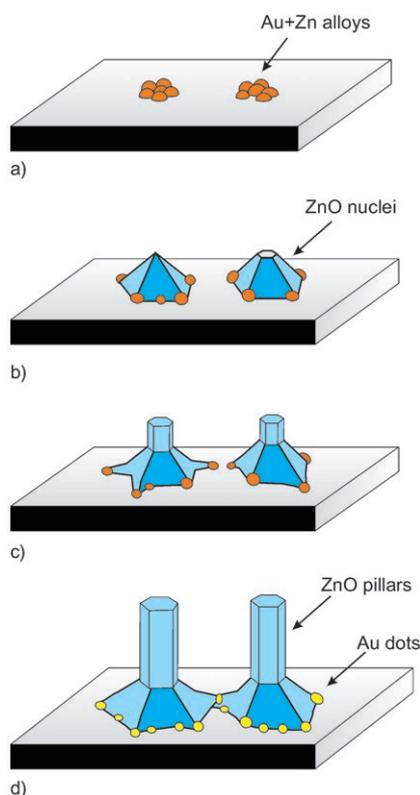
Figure 5. Schematic diagram of the growth process of the ZnO pillars. a) At elevated temperature Zn vapor atoms dissolve in gold fragments and form alloys. b) Precipitation and oxidation of Zn into (0001)-oriented quasi-hexagonal ZnO nuclei upon mergence. The central nuclei remain surrounded by the alloys. c) Zn atoms, at a high vapor concentration, migrate on the ZnO pyramids, nucleate at their peaks, and grow homoepitaxially into faceted short pillars. In the meantime, the small alloyed heads surrounding the nuclei can direct the in-plane growth of ZnO in the trails of their diffusion on the GaN surface. d) ZnO pillars after prolonged growth and cooling. Some of the pillars are joined at their bases due to extended in-plane growth and mergence. Au nanodots, precipitated from the alloys, remain surrounding the base of the pillars.

end of the small tube, which was located at an elevated temperature (800 °C) region. At the beginning of the growth, the original gold nanodisks (3 nm in thickness and ≈130 nm in diameter) fragmented into smaller particles, each absorbing Zn atoms to form alloyed liquids (see Figure 5a). The volume expansion of the alloys and their diffusion on the GaN surface led to coagulation into a larger droplet. Upon precipitation and oxidation of Zn, a central ZnO nucleus is formed. Due to an epitaxial relationship, the nuclei are quasi-hexagonal and [0001]-oriented pyramids (see Figures 4a and 5b). Diffusion of the fragments has been routinely observed in the vapor-phase growth of ZnO and In_2O_3 nanowires using thin gold films[17] or thin gold pads.[18]

Once a nucleus is formed, newly arrived Zn atoms impinge and migrate on the surface of the pyramid. They will finally nucleate and integrate into a ZnO lattice at the peaks of the pyramids that provide the lowest-energy sites. Zn atoms on the flat GaN surface migrate to the base of the

growing pillars or are desorbed. This is a similar vapor–solid (VS) process as the one we described previously.[7a] Following this VS process, ZnO tends to protrude from the center of the nuclei and grow into short pillars (Figures 4b and 5c). These well-faceted short pillars serve as preferential nucleation sites for further deposition of highly saturated Zn vapor and seeds for homoepitaxial growth of ZnO.

After continuous growth for 20 min, well-defined pillar structures were obtained (Figure 4c). These pillars are ≈180 nm in diameter and ≈1 µm in length, and cross-sectional TEM (data not shown) shows that the Au particles are mainly at their bases, and not at their tips. Compared to the thick (300 nm) and long (2 µm) pillars after a prolonged growth period of 40 min (see Figure 2), these pillars are short and thin, which implies that the vapor-phase growth of ZnO in a later stage occurs in both the lateral and vertical directions. This is a typical property of the VS growth of ZnO, which involves crystallographic-direction-dependent anisotropic growth. Due to the difference in surface energy of different crystal faces, the growth rate of hexagonal ZnO is faster in [0001] directions than those in [2$\bar{1}\bar{1}$0] and [10$\bar{1}$0]. Hence, the expected crystals are elongated along [0001]. A model of such a VS growth process is shown schematically in Figure 5c and d.

Meanwhile, in-plane ZnO VLS growth can also occur at the base of the pillars. It was directed by the diffusing Au nanoparticles away from the central nuclei, and resulted in (0001)-oriented ZnO stripes or 2D films via the VLS mechanism.[17] This can already be seen in the early growth stage (Figure 4a,b). Indeed, many tiny Au nanoparticles were observed at the edge of the central ZnO nuclei (indicated by arrows in Figure 4a1 and b1) and at the bases of thin pillars (see the bright spots in Figure 4c1). An extended 2D growth would give rise to more covering of the substrate surface, eventually leading to the interconnection of some pillars at their bases after a 40-min growth period (Figures 3a and 5d). The tiny Au particles observed in the cross-sectional TEM image (Figure 3c) could be the particles projected from the front and rear sides of the pillars' bases, since there is more than one row of the pillar array present in the TEM image.

On the basis of above description, the whole growth process of the pillars is a combination of the VLS and VS mechanisms: the former is responsible for the formation of (0001)-oriented ZnO nuclei at an early stage (as well as the in-plane growth of ZnO between the pillars), while the latter controls the subsequent anisotropic crystal growth that leads eventually to the 300-nm-wide, 2-µm-long pillars. The role of Au at temperatures (≈800 °C) higher than the melting point of Zn (420 °C) is to provide a thermodynamic low-energy interface with a sticking coefficient close to unity.[19] It is known that the VLS and VS processes can play competitive roles in the vapor-phase growth of nanostructures, depending on the vapor supersaturation and temperature.[20] With high vapor supersaturation and/or at high temperatures, VS growth can dominate over the VLS process. Under our experimental conditions, it is believed that the use of a small alumina tube facilitates an effective supersaturation of Zn, thus providing a high local vapor concen-

tration.[21] In addition, the deficiency of oxygen inside the small tube diminished the preoxidation of Zn atoms.[2d, 16] As a result, the vapor supersaturation of Zn was much increased compared to that in experiments where no small tube was used, thus favoring the VS process. In their gold-catalyzed growth of 120–200-nm In_2O_3 nanowires, Nguyen et al.[17a] observed that the nanowire thickens throughout the growth process, while the catalytic head remains relatively constant. This is also due, as they believed, to sidewall epitaxial deposition; that is, indium vapor atoms are directly incorporated into the solid surface of the nanowires.

A self-catalyzed VLS model has been adopted by several groups to explain the low-temperature (500–600 °C) growth of ZnO nanowires in which no other metal catalyst was involved.[16,22] In that model, a significant amount of liquid Zn is formed at the early stage. The liquid can act as a sink for further Zn vapor atoms and catalyze the growth of ZnO nanowires. This effect, however, seems to be negligibly small in our high-temperature (800 °C) growth experiments. Indeed, unlike Geng et al.[16] who obtained ZnO nanowires on a bare (i.e., without Au) Si substrate at 500–600 °C, we did not observe any growth of ZnO on bare substrates or non-Au covered areas (see Figure 4).

The main advantage of applying such a combined VS/VLS process is that one can grow large wires of narrow size distribution, and avoid the frequently observed growth of a set of several nanowires from one gold site.[2c] To our knowledge, it seems impossible to grow such large ZnO pillar arrays based solely on the VLS process.

2.3. Photoluminescence Properties

Low-temperature micro-PL spectra were measured to assess the optical quality of the ZnO pillars. Figure 6 shows typical micro-PL spectra recorded at different temperatures
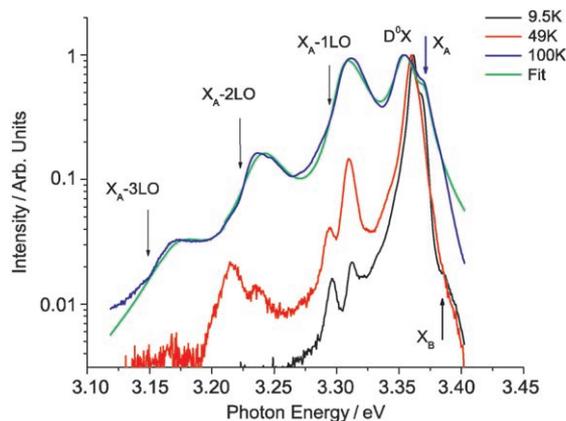

Figure 6. Micro-PL spectra of the ZnO pillars at different temperatures. $X_{A,B}$ and D^0X denote the free-exciton emission and the donor-bound exciton emission, respectively. At 100 K three pronounced phonon replicas of X_A are observed. The arrows indicate their energetic positions, which lie at the low-energy side of the X_A-LO peaks. A fit (green curve) to the spectrum at 100 K, which includes the typical lineshape of phonon side bands, confirms the unaltered energetic position of X_A (blue arrow) with respect to stress-free bulk ZnO.[26]

from 10 to 100 K. No PL lines from the GaN layer appear, as the excitation energy is chosen below the GaN bandgap. The strong peaks at 3.35–3.36 eV are attributed to neutral-donor-bound exciton lines (D^0X), and the high-energy shoulders to the free exciton ($X_{A,B}$) emissions. Due to the limited spectral resolution, only the envelope of multiple bound exciton lines is present and individual bound exciton transitions are not resolved. For the same reason the two peaks located around 3.3 eV in the lower-temperature spectra, which are likely phonon replicas of X_B and D^0X, cannot be identified unambiguously. The position of the X_A peak, which is visible in the spectrum at elevated temperatures, agrees within instrumental error with the corresponding values of bulk ZnO,[23] thus implying that the ZnO pillars are essentially free of stress.[24]

When the temperature was increased, the relative intensity of D^0X to X_A decreased accompanied by a red-shift. This finding is consistent with the previously reported PL properties of high-quality ZnO films and other 1D nano-structures,[4,6] thus supporting our assignment of the PL peaks. Additionally, longitudinal optical (LO) phonon replicas of X_A (X_A-iLO, $i=1,2,3$) become prominent at 100 K. Such behavior is a clear indication of high crystalline quality. The luminescence of the sample is bright up to room temperature, uniform, and scale independent. Furthermore, a decay time of ≈ 200 ps was found from the time-resolved measurements, which is comparable to that of other ZnO systems.[25] In contrast to thinner nanorods,[25] the decay rate only has a slight dependence on temperature. Finally, the deep-level green emission, which is known to be related to structural defects (e.g., oxygen vacancies), was very weak in the PL spectrum. The intensity ratio of the deep-level emission to the near-band-edge emissions is about 1:5, which is rather low. Based on these PL results, we conclude that our ZnO pillars have good optical characteristics and are hence well-suited for optical applications.

2.4. Piezoelectric Characterization

Due to its nonsymmetric crystal structure, ZnO is a typical piezoelectric material with potential application as a piezoelectric transducer. Our 300-nm-diameter, regularly patterned, equal-height pillars provide a suitable sample for piezoelectric characterization, as the PFM tip can easily capture the pillars and has good electrical contact on the flat (0001) top surface. Here, the highly doped GaN layer below the pillars provides the bottom electrode, whereas the conducting tip acts as the top electrode, as shown schematically in Figure 7a. Besides its good lattice matching to ZnO, the high electrical conductivity ($\approx 0.05\ \Omega$ cm) is another benefit of using GaN as the substrate in our study as it facilitates the PFM measurement.

Figure 7b shows a PFM signal-mapping image of part of the pillar array and a top view of the corresponding topography. The bright area in the image corresponds to positive piezoresponse signals, that is, detectable oscillations perpendicular to the plane of the sample surface. The uniform-contrast region between the pillars is the zero-signal regime.
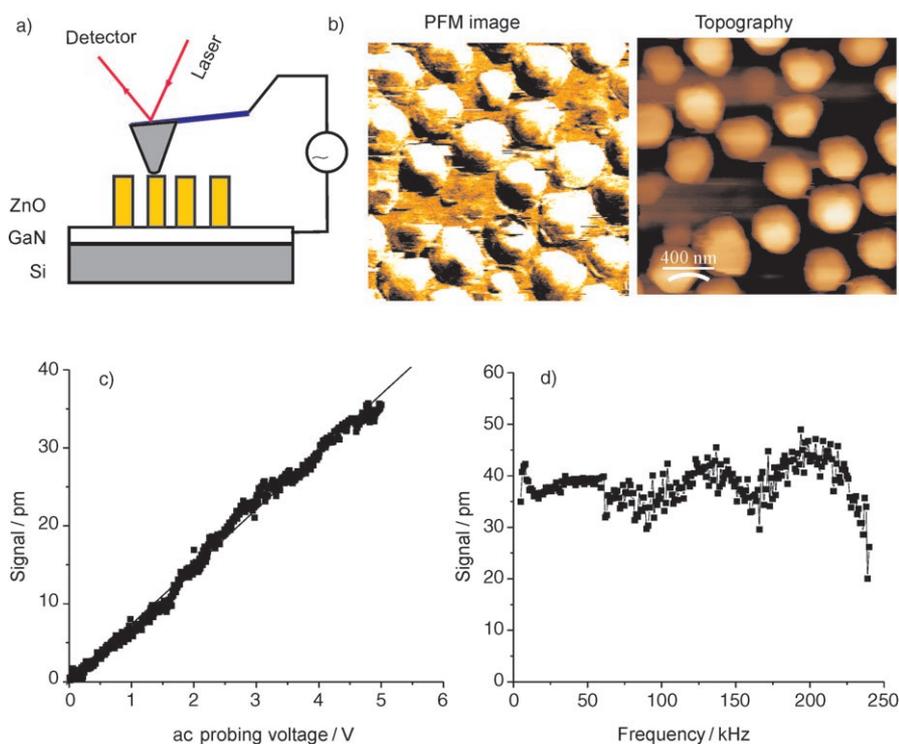
Figure 7. Piezoelectric characterization of the 300-nm ZnO pillars. a) Schematic diagram of the measurement setup. b) A typical scanning piezoresponse image showing that the piezoresponse signals originate selectively from the pillars (bright spots in the image). c) Measurement on an individual pillar with a probing frequency of 33.25 kHz. The piezoelectric coefficient d_{33} was determined to be (7.34 ± 0.3) pm V^{-1} from the slope of the linear fit. d) Frequency dependence of the piezoelectric signal at an ac probing signal of 5 V (RMS).

contribution of the cantilever to the entire PFM signal.[28] Recently, in their PFM measurements on ZnO nanobelts growing in the $[2\bar{1}\bar{1}0]$ direction, Zhao et al.[12] obtained a d_{33} value in the range 14.3–26.7 pm V^{-1}, which was strongly frequency dependent. The large difference could be partly due to the different sample geometries, that is, non-c-elongated nanobelts and c-elongated pillars, and partly due to the measurement geometry. In our case, a deliberately chosen cantilever was used to give a resonance frequency of the cantilever–sample system beyond 250 kHz, the frequency limit of our lock-in preamplifier.[28] Overall, our PFM result (effective coefficient and frequency independence of piezoresponse) implies that our pillars have nearly bulk properties in structure and piezoelectricity but contain a certain concentration of defects.

3. Conclusions

Large-area, overall hexagonally patterned ZnO nanopillars on a GaN/Si substrate have been fabricated by combining a template-assisted pattern definition procedure of the gold catalyst and vapor diffusion–deposition growth of ZnO. Based on TEM observations and a controlled time-sequenced growth study, the growth mechanism of the pillars appears to be a combination of vapor–liquid–solid and vapor–solid mechanisms. The former involves the formation of initial epitaxial ZnO nuclei on the gold sites, while the latter is responsible for the subsequent anisotropic crystal growth from highly supersaturated vapors. The pillars show strong excitonic emissions up to room temperature, which indicates a low defect density and good crystalline quality of the pillars. The piezoelectric behavior of the pillars shows a bulklike characteristic, that is, comparable effective piezoelectric coefficient and frequency independence of the piezoresponse. The different piezoelectric behavior of our pillars from that of belts could be due to their different sample structure. These nanopillars might be advantageous over nanowires and thin films of ZnO in a number of applications, for example, actuators and lasing cavities.

Compared to the topography, the piezoactive spots in the PFM image match exclusively the top of the pillars.

To study the piezoelectric coefficient and the frequency-dependent property of individual pillars, the tip was anchored at the piezoactive area chosen from either the topography image or the PFM signal-mapping image. The piezoelectric coefficient was measured by sweeping the applied ac voltage in the desired range. Figure 7c represents a typical example of the data, which gives an effective coefficient of 7.34 pm V^{-1}. Our measurements on tens of individual pillars gave similar results. The effective piezoelectric coefficient d_{33} averaged over all measurements is (7.5 ± 0.6) pm V^{-1}. This value is reasonable compared to the bulk values of (0001) ZnO measured by Christman et al.[11] (12.4 pm V^{-1}) and Zhao et al.[12] (9.93 pm V^{-1}) also using PFM. On the other hand, the value we obtained is still smaller than the bulk values. Piezoelectricity is known to be closely related to the sample structure, including symmetry, distortions, density of dislocations, etc.[27] Hence, the reduced electromechanical response might be an indication of a non-negligible number of structural defects in the pillars.

Figure 7d shows the dependence of the PFM signal on the probing frequency. The PFM signal is relatively flat over the measurement range of 0–230 kHz. This result is consistent with previous studies on the PFM method,[18] and the particular measurement geometry of the relatively high-aspect-ratio pillars, which minimize the linear electrostatic

© 2006 Wiley-VCH Verlag GmbH & Co. KGaA, D-69451 Weinheim

4. Experimental Section

The fabrication of the Au nanodisk template was reported in detail elsewhere.[13] The pillars were grown through a vapor diffusion–deposition process in a double-tube furnace system, as shown schematically in Figure 8. The source boat, loaded with a
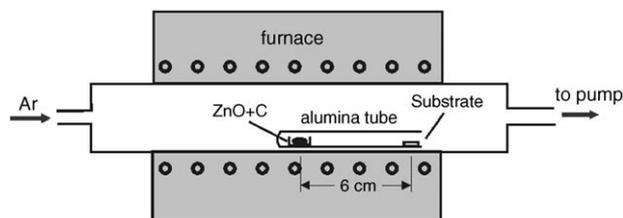

Figure 8. Schematic of the experimental setup for the growth of ZnO pillars. Both the source material and the substrate are placed inside a small alumina tube with a separation of about 6 cm.

mixture of powdered ZnO and graphite (1:1 wt%), and Au-coated substrate were placed in a small alumina tube inside a quartz-tube furnace (Carbolite). The distance between the source boat and substrate was typically 6 cm. The chamber was evacuated and back-flushed with Ar gas until the desired pressure of 200 mbar was reached. The whole system was elevated to the set temperature of 950 °C, maintained for specific times (40 min for the pillars in Figure 2), and then cooled naturally to room temperature. Due to the temperature gradient, the temperature at the substrate was measured as ≈ 800 °C. The thickness of the Au nanodisks deposited through the membrane mask was ≈ 3 nm.

SEM images were acquired using a JEOL JSM-6300F microscope (operating at 10 kV). High-resolution TEM and electron diffraction patterns were obtained on a JEOL JEM-4010 instrument (operating at 400 kV). The PL spectra were obtained using a time-resolved confocal micro-PL system (spatial resolution: ≤ 500 nm; temporal resolution: 5 ps). A frequency-doubled Ti:-sapphire laser was used to deliver ≈ 100-fs pulses at 3.49 eV with an average power of 250 µW. The sample was mounted in a He flow cryostat for temperature-dependent measurements. For the piezoelectric measurements by PFM (CP-Research, VEECO), a PtIr-coated Si tip was attached to a cantilever with an elastic constant of ≈ 3 N m^{-1} (ATEC-EFM, Nanosensors) and a resonant frequency of ≈ 300 kHz. The PFM system was previously calibrated at the same measurement frequency (33.25 kHz) by using an x-cut quartz wafer. The calibration was also verified from the force–distance curve of the AFM system. The downward force used to contact the wires was about 150 nN.

[1] For reviews, see: a) Y. Xia, P. Yang, Y. Sun, Y. Wu, B. Mayers, B. Gates, Y. Yin, F. Kim, H. Yan, *Adv. Mater.* **2003**, *15*, 353; b) G. C. Yi, C. Wang, W. I. Park, *Semicond. Sci. Technol.* **2005**, *20*, S22.

[2] a) P. Yang, H. Yan, S. Mao, R. Russo, J. Johnson, R. Saykally, N. Morris, J. Pham, R. He, H. J. Choi, *Adv. Funct. Mater.* **2002**, *12*, 323; b) H. J. Fan, F. Fleischer, W. Lee, K. Nielsch, R. Scholz, M. Zacharias, U. Gösele, A. Dadgar, A. Krost, *Superlattices Microstruct.* **2004**, *36*, 95; c) H. J. Fan, W. Lee, R. Scholz, A. Dadgar, A. Krost, K. Nielsch, M. Zacharias, *Nanotechnology* **2005**, *16*, 913; d) J. Song, X. Wang, R. Riedo, Z. L. Wang, *J. Phys. Chem. B* **2005**, *109*, 9869; e) X. Wang, J. Song, P. Li, J. H. Ryou, R. D. Dupuis, C. J. Summers, Z. L. Wang, *J. Am. Chem. Soc.* **2005**, *127*, 7920.

[3] M. Satoh, N. Tanaka, Y. Ueda, S. Ohshio, H. Saitoh, *Jpn. J. Appl. Phys. 2* **1999**, *38*, L586.

[4] a) W. I. Park, D. H. Kim, S. W. Jung, G. C. Yi, *Appl. Phys. Lett.* **2002**, *80*, 4232; b) W. I. Park, Y. H. Jun, S. W. Jung, G. C. Yi, *Appl. Phys. Lett.* **2003**, *82*, 964; c) W. I. Park, G. C. Yi, *Adv. Mater.* **2004**, *16*, 87.

[5] J. H. Choy, E. S. Jang, J. H. Won, J. H. Chung, D. J. Jang, Y. W. Kim, *Adv. Mater.* **2003**, *15*, 1911.

[6] a) Y. K. Tseng, C. J. Huang, H. M. Cheng, I. N. Lin, K. S. Liu, I. C. Chen, *Adv. Funct. Mater.* **2003**, *13*, 811; b) J. Jie, G. Wang, Y. Chen, X. Han, Q. Wang, B. Xu, J. G. Hou, *Appl. Phys. Lett.* **2005**, *86*, 031909.

[7] a) H. J. Fan, F. Bertram, A. Dadgar, J. Christen, A. Krost, M. Zacharias, *Nanotechnology* **2004**, *15*, 1401; b) M. Yan, H. T. Zhang, E. J. Widjajia, R. P. H. Chang, *J. Appl. Phys.* **2003**, *94*, 5240; c) Y. K. Tseng, C. T. Chia, C. Y. Tsay, L. J. Lin, H. M. Cheng, C. Y. Kwo, I. C. Chen, *J. Electrochem. Soc.* **2005**, *152*, G95.

[8] H. Chik, J. Liang, S. G. Cloutier, N. Kouklin, J. M. Xu, *Appl. Phys. Lett.* **2004**, *84*, 3376.

[9] a) X. Wang, C. J. Summers, Z. L. Wang, *Nano Lett.* **2004**, *4*, 423; b) D. Banerjee, J. Rybczynski, J. Y. Huang, D. Z. Wang, K. Kempa, Z. F. Ren, *Appl. Phys. A* **2005**, *80*, 749; c) H. J. Fan, B. Fuhrmann, R. Scholz, F. Syrowatka, A. Dadgar, A. Krost, M. Zacharias, *J. Cryst. Growth* **2006**, *287*, 34.

[10] E. C. Greyson, Y. Babayan, T. W. Odom, *Adv. Mater.* **2004**, *16*, 1348.

[11] J. A. Christman, R. R. Woolcott, Jr., A. I. Kingon, R. J. Nemanich, *Appl. Phys. Lett.* **1998**, *73*, 3851.

[12] M. H. Zhao, Z. L. Wang, S. X. Mao, *Nano Lett.* **2004**, *4*, 587.

[13] W. Lee, M. Alexe, K. Nielsch, U. Gösele, *Chem. Mater.* **2005**, *17*, 3325.

[14] R. S. Wagner, W. C. Ellis, *Trans. Metall. Soc. AIME* **1965**, *233*, 1053.

[15] L. Schubert, P. Werner, N. D. Zakharov, G. Gerth, F. M. Kolb, L. Long, U. Gösele, *Appl. Phys. Lett.* **2004**, *84*, 4968.

[16] C. Geng, Y. Jiang, Y. Yao, X. Meng, J. A. Zapien, C. S. Lee, Y. Lifshitz, S. T. Lee, *Adv. Funct. Mater.* **2004**, *14*, 589.

[17] a) P. Nguyen, H. T. Ng, T. Yamada, N. K. Smith, J. Li, J. Han, M. Meyyappan, *Nano Lett.* **2004**, *4*, 651; b) H. J. Fan, R. Scholz, M. Zacharias, U. Gösele, F. Bertram, D. Forster, J. Christen, *Appl. Phys. Lett.* **2005**, *86*, 023113.

[18] C. X. Xu, X. W. Sun, B. J. Chen, Z. L. Dong, M. B. Yu, X. H. Zhang, S. J. Chua, *Nanotechnology* **2005**, *16*, 70.

[19] a) T. Y. Tan, N. Li, U. Gösele, *Appl. Phys. Lett.* **2003**, *83*, 1199; b) K. A. Dick, K. Deppert, T. Martensson, B. Mandl, L. Samuelson, W. Seifert, *Nano Lett.* **2005**, *5*, 761.

[20] E. I. Givargizov, *Highly Anisotropic Crystals* (Ed.: M. Senechal), Reidel, Dordrecht, **1987**, p. 127.

[21] We also repeated the experiments under similar conditions without using the small alumina tube. No growth of ZnO was observed at all, and there was no obvious deposition of Zn onto gold.

[22] a) H. Y. Ding, J. Wang, S. S. Fan, *Nanotechnology* **2003**, *14*, 738; b) H. J. Fan, R. Scholz, F. M. Kolb, M. Zacharias, *Appl. Phys. Lett.* **2004**, *85*, 4142.

[23] a) Y. Harada, H. Kondo, N. Ichimura, S. Hashimoto, *Jpn. J. Appl. Phys. 2* **1999**, *38*, L1318; b) K. Ogata, T. Kawanishi, K. Maejima, K. Sakurai, S. Fujita, S. Fujita, *Jpn. J. Appl. Phys. 2* **2001**, *40*, L657.

[24] B. K. Meyer, H. Alves, D. M. Hofmann, W. Kriegseis, D. Forster, F. Bertram, J. Christen, A. Hoffmann, M. Straßburg, M. Dworzak, U. Haboeck, A. V. Rodina, *Phys. Status Solidi B* **2004**, *241*, 231.

[25] H. Priller, R. Hauschild, J. Zeller, C. Klingshirn, H. Kalt, R. Kling, F. Reuss, Ch. Kirchner, A. Waag, *J. Lumin.* **2005**, *112*, 173.

[26] S. Permogorov, in *Excitons* (Eds.: E. I. Rashka, M. D. Sturge), North-Holland, Amsterdam, **1982**, p. 177.

[27] *Nanoscale Characterization of Ferroelectric Materials—Scanning Probe Microscopy Approach* (Eds.: M. Alexe, A. Gruvermann), Springer, Berlin, **2004**.

[28] C. Harnagea, M. Alexe, D. Hesse, A. Pignolet, *Appl. Phys. Lett.* **2003**, *83*, 338.